Enhanced cytotoxic effect of camptothecin nanosponges in anaplastic thyroid cancer cells in vitro and in vivo on orthotopic xenograft tumors

Gigliotti, Casimiro Luca; Ferrara, Benedetta; Occhipinti, Sergio; Boggio, Elena; Barrera, Giuseppina; Pizzimenti, Stefania; Giovarelli, Mirella; Fantozzi, Roberto; Chiocchetti, Annalisa; Argenziano, Monica; Clemente, Nausicaa; Trotta, Francesco; Marchiò, Caterina; Annaratone, Laura; Boldorini, Renzo; Dianzani, Umberto; Cavalli, Roberta; Dianzani, Chiara. Enhanced cytotoxic effect of camptothecin nanosponges in anaplastic thyroid cancer cells in vitro and in vivo on orthotopic xenograft tumors. DRUG DELIVERY. 24 (1) pp: 670-680.
DOI: 10.1080/10717544.2017.1303856

Enhanced cytotoxic effect of Camptothecin nanosponges in anaplastic thyroid cancer cells *in vitro* and *in vivo* on orthotopic xenograft tumors

Casimiro Luca Gigliotti[1*], Benedetta Ferrara[2*], Sergio Occhipinti[3*], Elena Boggio[1], Giuseppina Barrera[4], Stefania Pizzimenti[4], Mirella Giovarelli[3], Roberto Fantozzi[2], Annalisa Chiocchetti[1], Monica Argenziano[2], Nausicaa Clemente[1], Francesco Trotta[5], Caterina Marchiò[6], Laura Annaratone[6], Renzo Boldorini[1], Umberto Dianzani[1], Roberta Cavalli[2], and Chiara Dianzani[2]

[1]*Department of Health Sciences, Interdisciplinary Research Center of Autoimmune Diseases, UPO, 28100 Novara, Italy,* [2]*Department of Drug Science and Technology, University of Torino, 10125 Torino, Italy,* [3]*Department of Molecular Biotechnology and Health Sciences, University of Torino, 10126 Torino, Italy,* [4] *Department of Clinical and Biological Sciences, University of Torino, 10043 Orbassano, Torino, Italy,* [5] *Department of Chemistry, University of Torino, 10125 Torino, Italy, and* [6]*Department of Medical Sciences, University of Torino, 10126 Torino, Italy*

[*]These authors have contributed equally.

Address for correspondence

Umberto Dianzani, Department of Health Sciences, Interdisciplinary Research Center of Autoimmune Diseases, University of Piemonte Orientale, 28100 Novara, Italy.

E-mail: umberto.dianzani@med.uniupo.it

Word Counts: 5102

Abstract

Anaplastic carcinoma of the thyroid (ATC) is a lethal human malignant cancer with median survival of 6 months. To date, no treatment has substantially changed its course, which makes urgent the need for development of novel drugs or novel formulations for drug delivery. Nanomedicine has enormous potential to improve the accuracy of cancer therapy by enhancing availability and stability, decreasing effective doses and reducing side effects of drugs.

Camptothecin (CPT) is an inhibitor of DNA Topoisomerase-I with several anticancer properties but has poor solubility and a high degradation rate. Previously, we reported that CPT encapsulated in ϐ-cyclodextrin-nanosponges (CN-CPT) increased solubility, was protected from degradation and inhibited the growth of prostate tumor cells both *in vitro* and *in vivo*. The aim of this study was to extend that work by assessing the CN-CPT effectiveness on ATC both *in vitro* and *in vivo*.

Results showed that CN-CPT significantly inhibited viability, clonogenic capacity and cell cycle progression of ACT cell lines showing a faster and enhanced effect compared to free CPT. Moreover, CN-CPT inhibited tumor cell adhesion to vascular endothelial cells, migration, secretion of pro-angiogenic factors (IL-8 and VEGF-α), expression of ϐ-PIX, belonging to the Rho family activators, and phosphorylation of the Erk1/2 MAPK.

Finally, CN-CPT significantly inhibited the growth, the metastatization and the vascularization of orthotopic ATC xenografts in SCID/beige mice without apparent toxic effects *in vivo*. This work extends the previous insight showing that ϐ-cyclodextrin nanosponges are a promising tool for treatment of ATC.

Keywords

Camptothecin, ϐ-cyclodextrin-nanosponges, anaplastic thyroid carcinoma, cell migration, cell adhesion.

Casimiro Luca Gigliotti *Department of Health Sciences, Interdisciplinary Research Center of Autoimmune Diseases, UPO, 28100 Novara, Italy* luca.gigliotti@med.uniupo.it Post-doc in Immunology Laboratory with expertise in tumor immunology.

Benedetta Ferrara *Department of Drug Science and Technology, University of Torino, 10125 Torino, Italy,* benedetta.ferrara@unito.it Ph student in the Parmacology Laboratory.

Sergio Occhipinti *Department of Molecular Biotechnology and Health Sciences, University of Torino, 10126 Torino, Italy* sergio.occhipinti@unito.it Post-doc in Immunology Laboratory with expertise in tumor immunology.

Elena Boggio *Department of Health Sciences, Interdisciplinary Research Center of Autoimmune Diseases, UPO, 28100 Novara, Italy* elena.boggio@med.uniupo.it Post-doc in Immunology Laboratory with expertise in tumor immunology.

Giuseppina Barrera *Department of Clinical and Biological Sciences, University of Torino, 10043 Orbassano, Torino, Italy* giuseppina.barrera@unito.it Associate Professor with expertise in Oncology and Pathology.

Stefania Pizzimenti *Department of Clinical and Biological Sciences, University of Torino, 10043 Orbassano, Torino, Italy* stefania.pizzimenti@unito.it Researcher with expertise in Oncology and Pathology.

Mirella Giovarelli *Department of Molecular Biotechnology and Health Sciences, University of Torino, 10126 Torino, Italy* mirella.giovarelli@unito.it Full Professor of Immunology with expertise in tumor immunology.

Roberto Fantozzi *Department of Drug Science and Technology, University of Torino, 10125 Torino, Italy,* roberto.fantazzi@unito.it Full Professor of Pharmacology with expertise in drug delivery.

Annalisa Chiocchetti *Department of Health Sciences, Interdisciplinary Research Center of Autoimmune Diseases, UPO, 28100 Novara, Italy* annalisa.chiocchetti@med.uniupo.it Researcher with expertise in Oncology and Pathology.

Monica Argenziano *Department of Drug Science and Technology, University of Torino, 10125 Torino, Italy,* monica.argenziano@unito.it Ph student with expertise in nanoparticles preparations

Nausicaa Clemente *Department of Health Sciences, Interdisciplinary Research Center of Autoimmune Diseases, UPO, 28100 Novara, Italy* nausicaa.clemente@med.uniupo.it Post-doc in Immunology Laboratory with expertise in mouse models.

Francesco Trotta *Department of Chemistry, University of Torino, 10125 Torino, Italy,* francesco.trotta@unito.it Full Professor of Chemistry with expertise in drug delivery

Caterina Marchiò *Department of Medical Sciences, University of Torino, 10126 Torino, Italy* caterina.marchio@unito.it Researcher of pathological anatomy with expertise in histology analyses.

Laura Annaratone *Department of Medical Sciences, University of Torino, 10126 Torino, Italy* laura.annaratone@unito.it Post-doc in Pathological Anatomy with expertise in histology analyses.

Renzo Boldorini *Department of Health Sciences, Interdisciplinary Research Center of Autoimmune Diseases, UPO, 28100 Novara, Italy* renzo.boldorini@med.uniupo.it Full Professor of Pathological Anatomy

Umberto Dianzani *Department of Health Sciences, Interdisciplinary Research Center of Autoimmune Diseases, UPO, 28100 Novara, Italy* umberto.dianzani@med.uniupo.it Full Professor of Immunology with expertise in tumor immunology and Cancer Research.

Roberta Cavalli *Department of Drug Science and Technology, University of Torino, 10125 Torino, Italy* roberta.cavalli@unito.it Full Professor of Chemistry with expertise in drug delivery.

Chiara Dianzani *Department of Drug Science and Technology, University of Torino, 10125 Torino, Italy,* chiara.dianzani@unito.it Researcher in Pharmacology with expertise in Cancer Research, Human Biology and Cell Biology.

Introduction

Thyroid cancers are the most common tumors of endocrine origin and their incidence has increased globally over the past 10 years (Jemal et al., 2011). They derive from follicular and para-follicular cells and most of them are differentiated papillary and follicular carcinomas, while 1% of cases are partly differentiated or undifferentiated and classified as anaplastic thyroid carcinoma (ATC). Most differentiated carcinomas display slow progression and are effectively treated with thyroidectomy and radioiodine ablation (Broecker-Preuss et al., 2015). By contrast, ATC progression is extremely rapid and no effective systemic therapy has been established so that the overall survival level is only 13% (Gilliland et al., 1997). At time of diagnosis, ATC often display an advanced stage of development, local invasion of the trachea, esophagus, blood vessels and muscles, and development of distant metastases to the mediastinum, lung, liver, bone and brain (Phay et al., 2013; Chen et al., 2014; Mirrielees et al., 2014; Varinot et al., 2014). Risk factors of thyroid cancers include environmental and genetic factors, exposure to ionizing radiation, and pre-existing thyroid neoplasia (Campanella et al., 2014). Genetic alterations that contribute to thyroid carcinoma include point mutations of BRAF and RAS (Fukushima & Takenoshita, 2005; Marotta et al., 2011); translocations involving RET/PTC1, RET/PTC3 and PAX8/PPAR-ɔ (Romei & Elisei, 2012; Raman & Koenig, 2014), and alterations of the DNA methylation pattern (Ragazzi et al., 2014; Faam et al., 2015).

To date, no effective therapies are available for ATC, which are currently treated with trivalent therapies including surgery, chemotherapy and radiotherapy resulting in an increased median survival of only 5 months (Wein & Weber, 2011; Parenti et al., 2014).

Camptothecin (CPT) is a pentacyclic alkaloid isolated from the bark of Campotheca Acuminata, (Wall et al., 1996). It quickly enters into cells and exerts anti-tumor activity by blocking topoisomerase-1 (TOP-1) in a specific and reversible manner. Unfortunately, it is weakly soluble in water and undergoes spontaneous and rapid inactivation at neutral pH by the opening of its six member lactone E ring. Therefore, it requires a prolonged infusion, so that the complex TOP-1 is

kept in place long enough to allow the induction of DNA damage (Fassberg & Stella, 1992; Chourpa et al., 1998). Moreover, its dosage and anti-tumor efficacy are limited by severe side effects, such as severe myelosuppression accompanied by prolonged diarrhea, fever, nausea and vomiting (Basili & Moro, 2009). The main water-soluble derivatives of CPT are the Irinotecan (Compostar®) and Topotecan (Hycamtin®).

To overcome problems in administering the drug, we previously investigated the antineoplastic effects of CPT- loaded into nanosponges of ß-cyclodextrin (CN-CPT) (Gigliotti et al., 2016a). Results showed that CN-CPT increased solubility, was protected from degradation and inhibited the growth of prostate tumor cells both in vitro and in vivo to a higher extent than free CPT. Cyclodextrin nanosponges are novel biocompatible polymer nanoparticles obtained by cross-linking of cyclodextrins (Subramanian et al., 2012), which are cyclic oligosaccharides consisting of multiple Ŭ-D-glucopyranose units linked together by an Ŭ-1.4 bond and include Ŭ, ß and ɔ cyclodextrins carrying six, seven or eight glucopyranose units, respectively. ß-cyclodextrin is the most widely used for nanosponge production because of its high capability to encapsulate drugs (Torne et al., 2013; Trotta et al., 2014).

The aim of this study was to extend that work by assessing the CN-CPT effectiveness on ATC both in vitro and in vivo. Results showed that CN-CPT inhibited the growth of ATC cell lines both in vitro and in vivo to a higher extent than free CPT. Moreover, it inhibited tumor cell adhesion to endothelial cells and migration which suggest that it may be effective also to inhibit tumor metastatic dissemination.

Methods

Materials

CPT was purchased from Sigma-Aldrich (Sigma-Aldrich, St Louis, MO, USA). ß-Cyclodextrins (ß-CDs) were a gift from Roquette (France). CD nanosponges (CNs) cross-linked at 1:4 molar ratio with carbonyldiimidazole were prepared as described previously (Swaminathan et al., 2010). All reagents were of analytical grade. Laboratory reagents were from Sigma-Aldrich unless otherwise specified. Cell culture reagents were purchased from Gibco/Invitrogen (Life Technologies, Paisley, UK) except where otherwise indicated.

Preparation of CPT in solution and camptothecin-loaded nanosponges (CN-CPT)

To prepare the CPT solution, about 1 mg of CPT was dissolved in 1 mL of dimethylsulfoxide (DMSO): water mixture (1:1, w/w) at pH = 5.5. A further dilution was carried out using 0.9 % NaCl solution at pH = 5.5 containing 30 % of DMSO.

To load CPT in CNs, 4 mg of CPT were added to an aqueous suspension of CNs in a ratio of 1:4 (drug to CN by weight) at pH 5.5 and stirred for 24 h in the dark. The aqueous suspension was then centrifuged at 8000 rpm for 10 min to separate the free drug, not incorporated, as a solid residue below the colloidal supernatant. The colloidal supernatant was freeze-dried to obtain drug-loaded nanosponges as a powder. This powder can be stored at 4 °C until use.

A weighed amount of freeze-dried CN-CPT was dispersed in a sterile aqueous solution at pH 6.0 containing 0.9 % NaCl and 3% polyethylene glycol (PEG)-400 w/v under stirring to obtain an isotonic aqueous nanosuspension containing 100 $\mu g \cdot mL^{-1}$ of CPT for the in vivo administration. For the free CPT formulation, a weighed amount of CPT was dissolved in a DMSO: water mixture (1:1, w/w) at pH = 5.5 and then diluted with a sterile aqueous solution at pH 6.0 containing 0.9 % NaCl and 3 % PEG-400 w/v to obtain a 100 $\mu g \cdot mL^{-1}$ concentration. The quantitative determination of CPT concentration in the formulations was evaluated by HPLC (Swaminathan et al., 2010).

CN-CPT sizes and polydispersity indices were measured by dynamic light scattering using a 90 Plus particle sizer (Brookhaven Instruments Corporation, USA) equipped with MAS OPTION particle sizing software. The measurements were made at a fixed angle of 90 ° for all samples. The samples were suitably diluted with filtered distilled water for every measurement. Zeta potential measurement was then carried out using an additional electrode in the same instrument. For zeta potential determination, samples were diluted with 0.1 mM KCl and placed in the electrophoretic cell, where an electric field of about 15 V/cm was applied.

The in vitro release was carried out using multi-compartment rotating cells with a dialysis membrane (Sartorius, cut off 12,000 Da). The donor phase consisted of CPT-nanosponge formulation in phosphate buffer at pH 7.4 (1 ml). The receiving phase consisted of phosphate buffer, pH 7.4. The receiving phase was completely withdrawn and replaced with fresh medium after fixed time intervals, suitably diluted and analyzed using the HPLC method described before.

CN-CPT showed an average diameter of about 350 nm, a polydispersity index of 0.11 and a negative surface charge with a zeta potential value of ï 27.4 mV. The in vitro release kinetics of CPT from nanosponge formulation was slow and prolonged over time, reaching 15.5 % after 24 h.

Cells

Human umbilical vein endothelial cells (HUVEC) were isolated from human umbilical veins by collagenase treatment (1%) and cultured in M199 medium with the addition of 20% fetal calf serum (FCS) 100 UI·mL^{-1} penicillin, 100 ε g·mL^{-1} streptomycin, 5 UI·mL^{-1} heparin, 12 ε g·mL^{-1} bovine brain extract and 200 mM glutamine. HUVEC were grown to confluence in flasks and used from the second to the fifth passage. Use of HUVEC was approved by the Ethics Committee of the óPresidio Ospedaliero Martiniô of Turin and conducted in accordance to the Declaration of Helsinki. Written informed consent was obtained from all donors.

The study was performed on two ATC cell lines, BHT-101 and CAL-62. Cells were purchased from Deutsche Sammlung von Mikroorganismen and Zellculturen (Braunschweig, Germany), which

certifies the origin and identity of the cells. The cell lines were grown in culture dishes as a monolayer in RPMI 1640 medium plus 10% FCS, 100 $U \cdot mL^{-1}$ penicillin, and 100 $\varepsilon g \cdot mL^{-1}$ streptomycin at 37 °C in a 5% CO_2 humidified atmosphere (Schweppe et al., 2008).

Cell viability assay

CAL-62 and BHT-101 ($1x10^3$/well) were seeded in 96-well plates and incubated at 37 °C, 5% CO_2, for 24 h. Then, cells were treated with different concentrations of CN-CPT or CPT ($2x10^{-10}$- $2x10^{-8}$M). After 24-48 h of incubation, viable cells were evaluated by 2,3-bis[2-methoxy-4-nitro-5sulphophenyl]-2H-tetrazolium-5carboxanilide (MTT) inner salt reagent at 570 nm, as described by the manufacturerôs protocol. The controls (i.e. cells that had received no drug) were normalized to 100%, and the readings from treated cells were expressed as % of viability inhibition. Eight replicates were used to determine each data point and five different experiments were performed.

Colony-Forming assay

CAL-62 and BHT-101 cells (800/well) were seeded into six-well plates and treated with the compounds (10^{-10}-10^{-8}M). The medium was changed after 72 h and cells were cultured for additional 10 days. Subsequently, cells were fixed and stained with a solution of 80% crystal violet and 20% methanol. Colonies were then photographed and counted with a Gel Doc equipment (Bio-Rad Laboratories, Hercules, CA, USA). Then, cells were washed and 30% acetic acid were added to induce a complete dissolution of the crystal violet. Absorbance was recorded at 595 nm by a 96-well-plate ELISA reader. Five different experiments were performed.

Cell adhesion assay

HUVEC were grown to confluence in 24-well plates. Then, they were pre-treated with increasing concentrations of CPT or CN-CPT (10^{-11}-10^{-8}M) for 24 h and washed twice with fresh medium. The tumor cells ($1x10^5$ cells/well) were seeded and left to adhere with HUVEC for 1 h, as previously

reported (Minelli et al., 2012a; Minelli et al., 2012b). Unattached tumor cells were washed away and the number of adherent cells was evaluated by the Image Pro Plus Software for micro-imaging (Media Cybernetics, version 5.0, Bethesda, MD, USA). Viability of the unattached cells was evaluated by the Trypan Blu test. Data are shown as percentage of the inhibition of treated cells versus the control adhesion measured on untreated cells; the control adhesion was 48 ± 4 cells per microscope field (n = 6) for BHT-101 cells and in a similar range (44 ± 5 cells) for CAL-62 (mean±SEM) (Dianzani et al., 2010).

Cell motility assay

In the wound healing assay, after starvation for 18-24 h in serum free medium, cells were plated onto six-well plates (10^6 cell/well) and grown to confluence. Cell monolayers were wounded by scratching with a pipette tip along the diameter of the well, and they were washed twice with serum-free medium before their incubation with culture medium in the absence or presence of CPT or CN-CPT (10^{-8}M) and mitomycin C (50 $\varepsilon g \cdot mL^{-1}$, Sigma-Aldrich). In order to monitor cell movement into the wounded area, five fields of each wound were photographed immediately after the scratch (0 h) and after 24 h (Gigliotti et al., 2016a; Dianzani et al., 2014).

In the Boyden chamber (BD Biosciences, San Jose, CA, USA) invasion assay, cells (8000) were plated onto the apical side of 50 $\mu g \cdot mL^{-1}$ Matrigel-coated filters (8.2 mm diameter and 0.5 µm pore size; Neuro Probe, Inc.; BIOMAP snc, Milan, Italy) in serum-free medium with or without increasing concentration of the drugs ($2x10^{-9}$-$2x10^{-8}$M). Medium containing 20% FCS was placed in the basolateral chamber as a chemo attractant. After 24 h, cells on the apical side were wiped off with Q-tips. Cells on the bottom of the filter were stained with crystal-violet and counted (five fields of each triplicate filter) with an inverted microscope. Data are shown as percentages of the inhibition of treated cells versus the control migration measured on untreated cells. Control migration was 52 ± 4 cells per microscope field (n = 5) for BHT-101 cells and 66 ± 5 for CAL-62. (Occhipinti et al., 2013).

ELISA assay

CAL-62 or BHT-101 cells ($1*10^5$/well) were plated in 24-well plates and treated with CPT or CN-CPT (10^{-11}-10^{-8}M) for 48 h. CPT and CN-CPT were replenished every 24 h (48 h culture: 24 + 24 h) without changing the culture medium. Cell-free supernatants were collected and concentrations of Interleukin-8 (IL-8), Vascular Endothelial Growth Factor α (VEGF-α), and Angiopoietin 2 were measured by ELISA according to the instructions of the manufacturers (IL-8, eBioscience, San Diego, CA, USA; VEGF-α and Angiopoietin 2, R&D Systems, Minneapolis, MN, USA). Absorbance was detected with a microplate reader (Bio-Rad Laboratories), and the Excel program was used to calculate the standard curve.

Protein extraction and Western blot analysis

Cells were seeded into six- well plates and treated for 48 h with CPT or CN-CPT (10^{-8}-10^{-9}M). CPT and CN-CPT were replenished every 24 h (48 h culture: 24 + 24 h) without changing the culture medium. Cells were then lysed in a buffer composed of 50 mM Tris-HCl pH 7.4, 150 mM NaCl, 5 mM EDTA, 1% sodium deoxycholate, 1% Nonidet P-40, phosphatase and a protease inhibitor cocktail. Cell lysates were cleared from insoluble fractions by high speed centrifugation, and protein concentration was determined with a commercially available kit (Bio Rad Laboratories), and measured with a spectrophotometer (Jasco Analytical Instruments, Easton, MD, USA). Proteins (40 µg) were loaded on 10% SDS- PAGE gels and transferred onto nitrocellulose membranes after electrophoresis. These were blocked by incubation for 1 h at room temperature with 5% nonfat milk dissolved in TBS-Tween 20. The membranes were then probed overnight with antibodies to ϐ-PIX (AdipoGen International, San Diego, CA, USA), pospho-Erk1,2 (Santa Cruz Biotechnology, Dallas, TX, USA), or ϐ-actin (Sigma-Aldrich) and, after 3 washes, incubated for 1 h with the HRP-conjugated secondary antibody (Sigma-Aldrich). Bands were detected by chemiluminescence, and densitometric analysis was performed with the Multi-Analyst software (version 1.1, Bio-Rad Laboratories).

Cell cycle analysis

Cells (1.5×10^5) were treated with CPT or CN-CPT as reported above. After 48 h, adherent and non-adherent cells were collected, washed in PBS and fixed in 75% ice cold ethanol and subsequently resuspended in a buffer containing 0.02 $mg\cdot mL^{-1}$ RNase A (Worthington Biochemical Corporation, Lakewood, NJ, USA), 0.05 $mg\cdot mL^{-1}$ propidium iodide (BD Biosciences), 0.2% v/v Nonidet P-40, 0.1% w/v sodium citrate. Samples were analyzed with a FACSCalibur cytometer (BD Biosciences).

Annexin V staining and caspase-3 activity

Cells ($1.5x10^5$) were treated with CPT or CN-CPT as reported above. After 48 h, they were stained with annexin V using the Annexin V Fluos kit (Beckton Dickinson) and analyzed by flow cytometry. Live cells were those not displaying shrunken/hypergranular morphology and unstained by Annexin V. Caspase-3 activity was assessed in cell lysates using a fluorimetric assay (MBL, Watertown, MA, USA) following the manufactureô instructions.

In vivo animal models and tumor growth

Animal studies were performed in accordance with EU and institutional guidelines approved by the Bioethics Committee for Animal Experimentation of the University of Turin, Italy (Prot. No. 4.2/2012) using NOD-SCID IL2Rƍ^{null} (NSG; 10/11-week-old female) mice, bred under sterile conditions in our animal facilities. Animals were anesthetized with intramuscular injection of Zoletil® (Zolaxepan and Tiletamina) and Rompun® (Xylazina). CAL62 cells were harvested from subconfluent cultures by trypsinization and washed in PBS. Then, cells (10^6 cells in 10 µl) were injected into the right thyroid lobe under surgical sterile conditions and tumors were allowed to grow during the following 10 days. Mice were then randomized into three groups receiving twice weekly intravenous injection of PBS (control group, n=5) or 1 $mg\cdot kg^{-1}$ CPT (n=7) or 1 $mg\cdot kg^{-1}$ CN-CPT (n=7).

Mice were weighed twice weekly and sacrificed when the animals appeared moribund. Tumor growth velocity (Tv) was determined using the formula: Tv = V / days from cells injection to excision.

Tumors and lungs were fixed in 10% formalin and paraffin embedded. Four serial sections/tumor were obtained and processed for immunohistochemistry using an automated slide processing platform (Ventana BenchMark XT AutoStainer, Roche) and a mouse monoclonal anti-human Ki-67 (Clone MIB-1) or a rabbit polyclonal anti-mouse CD31 (Abcam, Cambridge, UK) antibodies. Sections of lungs were stained with Hematoxylin and Eosin (H&E).

Ki-67 positive cells were heterogeneously distributed throughout the tumor. The Ki67 labeled nuclei were evaluated in the tumor areas where these markers were predominant (hot spots) using a digital camera (Olympus Q-colour 3) with area-based image analysis software (Dot-Slide 1.2 version). Ki-67 expression was calculated as the ratio between the labeled and the total nuclear areas. Only nuclei with a strongly positive label were counted. The ten fields with the highest density of positive nuclei were captured. A mean of 3,000 tumor cells per case (range, 2,000ï 3,800) was counted. Tumor microvessel density (TMD) was measured by evaluating the CD31-positive area and total tumor area per field upon after slide scan of the immunostaining as previously described (Gigliotti et al., 2016a; Passaro et al., 2016).

Data analysis

Data are shown as mean±standard error of the mean (SEM). Statistical analyses were performed with GraphPad Prism 5.0 software (San Diego, CA, USA). For the in vivo experiments, the results are expressed as the median with interquartile range. One way ANOVA was performed, followed by Tukeyôs multiple comparison post-test when needed. Kaplan-Mayer survival curves were evaluated with the Log Rank Mantel-Cox test. Only P values < 0.05 were considered to be significant.

Results

CN-CPT inhibits cell proliferation in vitro

We compared the ability of CN-CPT and free CPT to inhibit the growth of BHT-101 and CAL-62 in vitro. Cells were cultured in the presence and absence of titrated amounts ($2x10^{-10}$ - $2x10^{-8}$ M) of each compound for 24ï 48 h and the amount of viable cells was then assessed by the MTT assay. Figure 1 shows that CN-CPT inhibited the growth of both cell lines to a higher extent than CPT. The effect was concentration- and time-dependent with small differences between the two cell lines. The different effect of the two compounds was detectable in terms of timing, maximal inhibition, and effective doses.

To validate these findings, we performed clonogenic survival assays. Cells were seeded onto 6-well plates and treated with titrated doses (10^{-10}-10^{-8}) of each compound. The culture medium was changed after 72 h, and cells were cultured for 10 additional days in the absence of the compounds. Results showed that treatment with CN-CPT inhibited the ability to form colonies of both cell lines to a higher extent than CPT (supporting information, Figure S1**)**. The effect was concentration-dependent with small differences between the two cell lines. The different effect of the two compounds was detectable in terms of effective doses but not in terms of maximal inhibition that was similar at the highest dose.

To assess whether inhibition of cell proliferation induced by CN-CPT affected cell cycle progression, we analyzed the cell cycle in CAL-62 and BHT-101 cells cultured in the presence and absence of titrated amounts of CN-CPT or CPT (10^{-9} and 10^{-8} M) for 48 h. Results showed that both doses of CN-CPT induced a substantial accumulation of cells in S phase compared to the untreated control in both cell lines. This effect was exerted also by CPT but only at the highest dose (Figure 2).

To assess whether inhibition of cell proliferation induced by CN-CPT involved cell death, we analyzed Annexin V staining, detecting both apoptotic and necrotic cells, and caspase 3 activation,

detecting apoptosis, in CAL-62 and BHT-101 cells cultured in the presence and absence of titrated amounts (10^{-9} and 10^{-8} M) of CN-CPT or CPT for 48 h. Results showed that CN-CPT induced higher Annexin V staining and caspase 3 activation than CPT in both cells lines (Figure 3).

CN-CPT inhibits cell adhesion and migration in vitro

Adhesion of tumor cells to the vascular endothelium and their release into the bloodstream is a key step for metastasis formation (Ma & Waxman, 2008). Therefore, we performed in vitro experiments comparing the effect of CN-CPT and CPT on adhesion to HUVEC and motility of tumor cells.

In the adhesion experiments, HUVEC were pretreated for 24 h with titrated doses (10^{-11} and 10^{-8} M) of CN-CPT and CPT, washed, and used for adhesion assays with CAL-62 and BHT-101 cells. Results showed that CN-CPT inhibited adhesion of both cell lines at higher levels than CPT. The effect was concentration-dependent with small differences between the two cell lines. The different effect of the two compounds was detectable in terms of both effective doses and maximal inhibition (Figure 4 A-B). The difference was not due to an effect on cell viability since cells were still alive after the 24 h incubation with the drug.

Cell motility was initially assessed using a wound healing assay evaluating cell random migration. A linear scratch was done in confluent monolayers of CAL-62 and BHT-101 cells, which were then cultured in FCS-free medium to minimize cell proliferation in the presence or absence of CN-CPT and CPT (10^{-8} M). Analysis of the cell ability to migrate into the scratch after 24 h showed that CN-CPT inhibited adhesion of both cell lines at higher levels than CPT (supporting information, Figure S2). Then, cell motility was assessed using a Boyden chamber assay assessing directional migration of cells. CAL-62 and BHT-101 cells were seeded in the upper chamber of a Boyden chamber in serum-free medium in the presence or absence of titrated doses ($2x10^{-9}$ and $2x10^{-8}$ M) of CN-CPT and CPT and allowed to migrate for 24 h toward the lower chamber containing medium with and without 20% FCS, used as a chemoattractant. Results showed that CN-CPT inhibited cell migration at higher levels than CPT in both cell lines (Figure 4 C-D). The CN-CPT effect was concentration-

dependent with small differences between the two cell lines, whereas CPT displayed some effect on CAL-62 cells but it was almost ineffective on BHT-101 cells.

In both migration assays, doses and timing of treatments minimized the possible confounding effects due to the drug effect on cell growth.

CN-CPT inhibits VEGF-α and IL-8 secretion in vitro.

Since ATC cells express high levels of pro-angiogenic molecules (Passaro et al., 2016; Jayasooriya et al., 2011), we evaluated the effect of the drugs on secretion of VEGF-α, IL-8, and Angiopoietin 2. CAL-62 and BHT-101 cells were incubated with titrated doses (10^{-11}-10^{-8} M) of CN-CPT or CPT for 48 h. Then, secretion of VEGF-α, IL-8, and Angiopoietin 2 was evaluated by ELISA in the culture supernatants. Results showed that the ATC cells produced a substantial amount of these factors and CN-CPT inhibited the secretion of VEGF-α and IL-8 compared to the free drug at the same concentrations (supporting information, Figure S3). No differences were found for Angiopoietin 2 secretion (data not shown).

CN-CPT inhibits ϐ-PIX expression and $ERK_{1,2}$ phosphorylation in vitro

In order to investigate the mechanisms underlying CN-CPT mediated inhibition of cell proliferation, adhesion, and migration, we evaluated the effect of the drug on expression of ϐ-PIX, involved in rearrangement of the cytoskeleton and cell migration, and on Erk1,2 phosphorylation involved in signaling of multiple surface receptors (Kim et al., 2013; Occhipinti et al., 2013; Dianzani et al., 2014; Stevens et al., 2014; Gigliotti et al., 2016b). CAL-62 and BHT-101 cells were incubated with titrated doses (10^{-9} and 10^{-8} M) of CN-CPT or CPT for 48 h, lysed, and analyzed for ϐ-PIX expression and Erk1,2 phosphorylation by Western blot. Results showed that CN-CPT inhibited ϐ-PIX expression and Erk1,2 phosphorylation at higher levels than CPT in both cell lines (Figure 5).

In vivo studies

We compared the effect of CN-CPT and CPT tumor growth and metastatic dissemination in NSG mice injected orthotopically in the thyroid lobe with CAL-62 cells and treated 10 days later with twice weekly injections of PBS, CPT or CN-CPT in the tail vein. Results showed that the overall survival of mice treated with CN-CPT was higher than that displayed by mice injected with either PBS or CPT (Figure 6A). In particular, median survivals of mice treated with PBS, CPT and CN-CPT were 28, 25 and 38 days, respectively. The difference of survival between the CN-CPT group and the control group was significant (P = 0.0422, log-rank test).

Analysis of tumor growth velocity showed that CN-CPT significantly inhibited the growth velocity of orthotopic anaplastic thyroid carcinoma xenografts compared to the control group, whereas CPT had no effect (Figure 6B).

Analysis of lung metastases showed that CN-CPT significantly inhibited development metastases compared to the control group whereas CPT had no effect (Figure 6C).

Histologic analysis of the primary tumor showed that, in control mice, the tumors displayed diffuse necrosis whereas, in CN-CPT-treated mice, tumors displayed decreased necrosis, and in CPT-treated mice an intermediate picture. Immunohistochemical staining, performed 34 days after tumor challenge showed that Ki-67^{+} cells were homogeneously distributed in the tumor mass in PBS- and CPT-treated mice, whereas, they were concentrated at the invasive edge in the peripheral area of the tumor, but rare in the centre of the tumor, in CN-CPT treated mice (Figure 6D). This enrichment of $Ki67^{+}$ cells was detected also at 51 days after tumor challenge (Figure 6E). To assess the effects on tumor angiogenesis, we stained the tumor sections for CD31 and evaluated the TMD. Results showed that treatment with CN-CPT substantially decreased the TMD compared with untreated mice and CPT-treated mice, whereas CPT had no effect (Figure 6 F).

All treatments were well tolerated by the animals without significant weight loss in any group.

Discussion

ATC is a highly aggressive tumor with a poor prognosis and the long-term survival is extremely rare. To date, available therapies do not significantly improve the survival of patients and have only a palliative effect (Patel & Shaha, 2006; Cornett et al., 2007).

CPT belongs to the drug category of inhibitors of DNA TOP-1 by specifically blocking TOP-1 during the cleavage reaction of DNA and preventing repair of the single-strand breaks. This effect

produces blocking of cells in the S phase of the cell cycle, conversion of DNA breaks from single to double helix and death of cells by apoptosis (Huang et al., 2000; Desai et al., 2001; Minelli et al., 2012a). Several studies demonstrated CPT activity in tumors of various origins, but CPT did not reach clinical use because of its numerous side effects. Moreover, its use is restricted by poor solubility and stability at physiological pH, at which CPT undergoes spontaneous inactivation due to opening of the E ring, decreased bioavailability and enhanced side effects. Several strategies have been described to improve the CPT activity and to decrease the side effects in several type of cancers (Acevedo-Morantes et al., 2013; Xie et al., 2016; Yang et al., 2016).

Previously, we have reported that CN-CPT displays increased solubility, is protected from degradation and displays an enhanced inhibitory effect on prostate tumor cells both in vitro and in vivo (Fassberg & Stella, 1992; Chourpa et al., 1998; Minelli et al., 2012a; Minelli et al., 2012b; Gigliotti et al., 2016a).

This work extends those observations to ATC showing that CN-CPT displays increased inhibitory effects in vitro on cell proliferation, as assessed by the MTT and clonogenic assay, and increased ability to block the cell cycle into the S phases and to induce apoptosis. These effects may be ascribable to the inhibitory activity of CPT on TOP1. Moreover, a role may be played also by inhibition of ERK 1,2 phosphorylation since constitutive activation of MAPK signalling is involved in cell survival and proliferation in several cancers, including thyroid cancer (Perri et al., 2015; Lim & Cha, 2011). It is noteworthy that inhibitors of the MAPK pathway may increase the efficacy of radioiodine therapy in cancer with BRAF mutations (Knauf & Fagin, 2009).

The in vitro experiments demonstrated that CN-CPT also shows increased ability to inhibit endothelial cells adhesiveness to ATC cells and migration of ATC cells, similarly to what we previously showed for prostate cancer cells. This activity might be related to the ability of CN-CPT to downmodulate expression of β-Pix involved in negative regulation of formation of focal adhesions, which may enhance formation of lamellipodia and cell motility (Kim et al., 2013; Occhipinti et al., 2013; Dianzani et al., 2014; Stevens et al., 2014).

The in vivo experiments using the SCID xenograft orthotopic model implanted with CAL-62 cells substantially supported these findings since treatment with CN-CPT was more effective than the free drug in improving mice survival and decreasing tumor growth and metastatization at a dose (1 $mg \cdot kg^{-1}$) that did not display any substantial side effects.

Beside the effect on cell proliferation, apoptosis, adhesion and migration, the anti-tumor CN-CPT activity may also involve inhibition of tumor neoangiogenesis as suggested by the CN-CTP ability to inhibit VEGF-α and IL-8 secretion in ATC cells lines in vitro and tumor vascularization in vivo. We previously showed that CN-CPT, but not free CPT, inhibits proliferation and migration of endothelial cells, proteolytic degradation of the extracellular matrix, and in several in vitro models of angiogenesis, inhibited tumor neoangiogenesis in mouse models of prostate cancer (Gigliotti et al., 2016a). Solid tumors cannot grow beyond a certain size, generally 1-2 mm^3, without being supported by tumor neoangiogenesis (Li et al., 2012), that plays a key role also for metastatic dissemination of cancer cells. Another point is that the higher in vivo activity of CN-CPT compared to free CPT may be partly due to its ability, displayed by most nanoparticles, to accumulate in tumors because of the enhanced permeation and retention effect across the atypical highly fenestrated blood vessels of the tumor (Wang & Thanou, 2010).

The greater size of the necrotic core detected in the tumors of the control group compared to those of the CN-CPT treated group may be ascribed to the faster growth of the former that may prevent adequate nutrition of the tumor core. The finding that the tumors of CN-CPT treated mice contained a high density of $Ki67^+$ cells at the invasive edge suggests that the anti-proliferative activity of the drug has limited effects in this area of the tumor. However, the CN-CPT effect might be potentiated by combination of CN-CPT with surgery and radiation, since the multimodality approach represents the standard treatment of choice in ATC (Denaro et al., 2013) and the striking CN-CPT effect on tumor metastatization may be crucial to implement the effect of those therapies. The safety (Gigliotti et al., 2016a) and the cheap cost of CN-CPT are also to be considered.

Conclusion

In conclusion, the antineoplastic activity of CN-CPT may result from the combination of the antiproliferative effect associated with the increase of apoptosis in the tumor cells, the inhibition of migration, invasion and metastatization, and~~, possibly,~~ the inhibition of the neoplastic neovascularisation. Therefore, the anticancer activity of CN-CPT, without evident toxicity, opens up therapeutic perspectives for the ATC, which doesnôt respond to conventional therapy. Translational and clinical studies will ultimately determine the clinical utility and safety of CN-CPT, used alone or in combination with other chemotherapics, as an option for the treatment of this kind of tumor.

Declaration of interest

The authors report no conflicts of interest. This work was supported by the University of Turin 2014 (ex 60% by G.B., R.C., and C.D.), by Fondazione Amici di Jean, and Associazione Italiana Ricerca sul Cancro (IG 14430, AIRC, Milan).

References

Acevedo-Morantes CY, Acevedo-Morantes MT, Suleiman-Rosado D, Ramírez-Vick JE (2013). Evaluation of the cytotoxic effect of camptothecin solid lipid nanoparticles on MCF7 cells. Drug Deliv. 20:338-48.

Basili S, Moro S (2009). Novel camptothecin derivatives as topoisomerase I inhibitors. Expert Opin Ther Pat 19:555-74.

Broecker-Preuss M, Müller S, Britten M, et al. (2015). Sorafenib inhibits intracellular signaling pathways and induces cell cycle arrest and cell death in thyroid carcinoma cells irrespective of histological origin or BRAF mutational status. BMC Cancer 15:184.

Campanella P, Ianni F, Rota CA, et al. (2014). Quantification of cancer risk of each clinical and ultrasonographic suspicious feature of thyroid nodules: a systematic review and meta-analysis. Eur J Endocrinol 170:R203-11.

Chen ED, Cheng P, Yan XQ, et al. (2014). Metastasis of distal esophageal carcinoma to the thyroid with presentation simulating primary thyroid carcinoma: a case report and review of the literature. World J Sur Oncol 12:106.

Chourpa I, Riou JF, Millot JM, et al. (1998). Modulation in kinetics of lactone ring hydrolysis of camptothecins upon interaction with topoisomerase I cleavage sites on DNA. Biochemistry 37:7284-91.

Cornett WR, Sharma AK, Day TA, et al. (2007). Anaplastic thyroid carcinoma: an overview. Curr Oncol Rep 9:152-58.

Denaro N, Nigro CL, Russi EG, Merlano MC (2013). The role of chemotherapy and latest emerging target therapies in anaplastic thyroid cancer. OncoTarget and therapy 6:1231-41.

Desai SD, Li TK, Rodriguez-Bauman A, et al. (2001). Ubiquitin/26S proteasome-mediated degradation of topoisomerase I as a resistance mechanism to camptothecin in tumor cells. Cancer Res 61:5926-32.

Dianzani C, Minelli R, Mesturini R, et al. (2010). B7h triggering inhibits umbilical vascular endothelial cell adhesiveness to tumor cell lines and polymorphonuclear cells. J Immunol 185:3970-79.

Dianzani C, Minelli R, Gigliotti CL, et al. (2014). B7h triggering inhibits the migration of tumor cell lines. J Immunol 192:4921-31.

Faam B, Ghaffari MA, Ghadiri A, Azizi F (2015). Epigenetic modifications in human thyroid cancer. Biomed Rep 3:3-8.

Fassberg J, Stella VJ (1992). A kinetic and mechanistic study of the hydrolysis of camptothecin and some analogues. J Pharm Sci 81:676-84.

Fukushima T, Takenoshita S (2005). Roles of RAS and BRAF mutations in thyroid carcinogenesis. J Med Sci 51:67-75.

Gigliotti CL, Minelli R, Cavalli R, et al. (2016 a). In Vitro and In Vivo Therapeutic Evaluation of Camptothecin-Encapsulated ß-Cyclodextrin Nanosponges in Prostate Cancer . J Biomed Nanotechnol 12:114-27.

Gigliotti CL, Boggio E, Clemente N, et al. (2016 b). ICOS-Ligand Triggering Impairs Osteoclast Differentiation and Function In Vitro and In Vivo. J Immunol 197:3905-16.

Gilliland FD, Hunt WC, Morris DM, Key CR (1997). Prognostic factors for thyroid carcinoma. A population-based study of 15,698 cases from the Surveillance, Epidemiology and End Results (SEER) program 1973-1991. Cancer 79:564-73.

Huang TT, Wuerzberger-Davis SM, Seufzer BJ, et al. (2000). NF-kappaB activation by camptothecin. A linkage between nuclear DNA damage and cytoplasmic signaling events. J Biol Chem 275:9501-09.

Jayasooriya RG, Park SR, Choi YH, et al. (2011) Camptothecin suppresses expression of matrix metalloproteinase-9 and vascular endothelial growth factor in DU145 cells through PI3K/Akt-mediated inhibition of NF-əB activity and Nrf2-dependent induction of HO-1 expression. Environ Toxicol Pharmacol. 39:1189-98.

Jemal A, Bray F, Center MM, et al. (2011). Global cancer statistics. CA Cancer J Clin 61:134.

Kim YS, Noh MY, Kim JY, et al. (2013). Direct GSK-3ɓ inhibition enhances mesenchymal stromal cell migration by increasing expression of ɓ-PIX and CXCR4. Mol Neurobiol 47:811-20.

Knauf JA, Fagin JA, Curr (2009). Role of MAPK pathway oncoproteins in thyroid cancer pathogenesis and as drug targets. Opin Cell Biol 21:296-303.

Li J, Chen F, Cona MM, et al. (2012). A review on various targeted anticancer therapies. Targ Oncol 7:69-85.

Lim YC, Cha YY (2011). Epigallocatechin-3-gallate induces growth inhibition and apoptosis of human anaplastic thyroid carcinoma cells through suppression of EGFR/ERK pathway and cyclin B1/CDK1 complex. J Surgical Oncology 104:776-80.

Ma J, Waxman DJ (2008). Combination of antiangiogenesis with chemotherapy for more effective cancer treatment. Mol Cancer Ther 7:3670-84.

Marotta V, Guerra A, Sapio MR, Vitale M (2011). RET/PTC rearrangement in benign and malignant thyroid diseases: a clinical standpoint. Eur J Endocrinol 165:499-507.

Minelli R, Cavalli R, Ellis L, et al. (2012 a). Nanosponge-encapsulated camptothecin exerts anti-tumor activity in human prostate cancer cells. Eur J Pharm Sci 47:686-94.

Minelli R, Serpe L, Pettazzoni P, et al. (2012 b). Cholesteryl butyrate solid lipid nanoparticles inhibit the adhesion and migration of colon cancer cells. Br J Pharmacol 166:587-601.

Mirrielees JA, Kapur JH, Szalkucki LM, et al. (2014). Metastasis of primary lung carcinoma to the breast: a systematic review of the literature. J Surg Res 188:419-31.

Occhipinti S, Dianzani C, Chiocchetti A, et al. (2013). Triggering of B7h by the ICOS modulates maturation and migration of monocyte-derived dendritic cells. J Immunol 190:1125-34.

Parenti R, Salvatorelli L, Magro G (2014). Anaplastic Thyroid Carcinoma: Current Treatments and Potential New Therapeutic Options with Emphasis on TfR1/CD71. Int J Endocrinol 685396.

Passaro C, Borriello F, Vastolo V, et al., (2016) The oncolytic virus dl922-947 reduces IL-8/CXCL8 and MCP-1/CCL2 expression and impairs angiogenesis and macrophage infiltration in anaplastic thyroid carcinoma. Oncotarget. 7:1500-15.

Patel KN, Shaha AR (2006). Poorly differentiated and anaplastic thyroid cancer. Cancer Control 13:119-28.

Perri F, Pezzullo L, Chiofalo MG, et al. (2015). Targeted therapy: A new hope for thyroid carcinomas. Critical Reviews in Oncology/Hematology 94:55ï 63.

Phay JE, Ringel MD (2013). Metastatic mechanisms in follicular cell-derived thyroid cancer. Endocr Relat Cancer 20:R307-19.

Ragazzi M, Ciarrocchi A, Sancisi V, et al. (2014). Update on anaplastic thyroid carcinoma: morphological, molecular, and genetic features of the most aggressive thyroid cancer. Int J Endocrinol 790834.

Raman P, Koenig RJ (2014). Pax-8-PPAR-ɔ fusion protein in thyroid carcinoma. Nat Rev Endocrinol 10:616-23.

Romei C, Elisei R (2012). RET/PTC Translocations and Clinico-Pathological Features in Human Papillary Thyroid Carcinoma. Front Endocrinol 3:54.

Schweppe RE, Klopper JP, Korch C, et al. (2008). Deoxyribonucleic acid profiling analysis of 40 human thyroid cancer cell lines reveals cross-contamination resulting in cell line redundancy and misidentification. J Clin Endocrinol Metab 93:4331-41.

Stevens BM, Folts CJ, Cui W, et al. (2014). Cool-1-mediated inhibition of c-Cbl modulates multiple critical properties of glioblastomas, including the ability to generate tumors in vivo. Stem Cells 32:1124-35.

Subramanian S, Singireddy A, Krishnamoorthy K, Rajappan M (2012). Nanosponges: a novel class of drug delivery system-review. J Pharm Pharm Sci 15:103-11.

Swaminathan S, Pastero L, Serpe L, et al. (2010). Cyclodextrin-based nanosponges encapsulating camptothecin: physicochemical characterization, stability and cytotoxicity. Eur J Pharm Biopharm 74:193-201.

Torne S, Darandale S, Vavia P, et al. (2013). Cyclodextrin-based nanosponges: effective nanocarrier for tamoxifen delivery. Pharm Dev Technol 18:619-25.

Trotta F, Dianzani C, Caldera F, et al. (2014). The application of nanosponges to cancer drug delivery. Expert Opin Drug Deliv 11:931-41.

Varinot J, Ménégaux F, Bitker MO, Compérat E (2014). Renal metastasis from thyroid carcinoma: a case report. Anal Quant Cytopathol Histpathol 36:46-50.

Wall ME, Wani MC, Cook CE, et al. (1966). Plant antitumor agent I: The isolation and structure of camptothecin, a novel alkaloidal leukemia and tumor inhibitor from Camptotheca acuminate. J Am Chem 88:3888-90.

Wang M, Thanou M (2010). Targeting nanoparticles to cancer. Pharmacological research 62:90-9.

Wein RO, Weber RS (2011). Anaplastic thyroid carcinoma: palliation or treatment? Curr Opin Otolaryngol Head Neck Surg 19:113-18.

Xie X, Lin W, Liu H et al., (2016) Ultrasound-responsive nanobubbles contained with peptide-camptothecin conjugates for targeted drug delivery. Drug Deliv. 23:2756-64.

Yang A, Liu Z, Yan B, et al., (2016) Preparation of camptothecin-loaded targeting nanoparticles and their antitumor effects on hepatocellular carcinoma cell line H22. Drug Deliv. 23:1699-706.

Figure Captions

Figure 1 Inhibition of cell viability following CPT or CN-CPT treatments. CAL-62 (A, B) or BHT-101 (C, D) cells ($1x10^3$/well) were treated with the indicated concentrations of drug for 24ï 48 h. Results are expressed as % of viability inhibition of control and shown as mean ± SEM (n = 5). *p<0.05, **p<0.01 significantly different from the same concentration of CPT.

Figure 2 Induction of cell cycle arrest by CPT or CN-CPT treatment. CAL-62 (A, B) and BHT-101 (C, D) cells ($1.5x10^5$) were treated or not with CPT or CN-CPT (10^{-8} and 10^{-9} M) for 48 h and cell

cycle was then assessed by flow cytometry. CPT and CN-CPT were replenished every 24 h (48 h culture: 24 + 24 h) without changing the culture medium. Graphs show: (A, C) the % of cells in each cycle phase detected in one representative experiment, (B, D) the % of cells in S phase cycle expressed as means ± SEM (n = 3). Each experiment was performed in triplicate. §§ $p<0.01$, significantly different from untreated cells; *$p<0.05$, **$p< 0.01$, significantly different from treated cells at the same drug concentration.

Figure 3 Proportions of Annexin-V positive cells and levels of caspase-3 activity after CPT or CN-CPT treatment. Annexin-V positive cells (A, B) and caspase-3 activity (C, D) was evaluated in CAL-62 (A, C) and BHT-101 (B, D) cells cultured for 48 h in the presence or absence of CPT or CN-CPT. CPT and CN-CPT were replenished every 24 h (48 h culture: 24 + 24 h) without changing the culture medium. Results are expressed as % of Annexin V positive cells and relative caspase activity %, calculated as result displayed by each treatment / the results displayed by untreated cells (n = 5). §$p< 0.05$; §§$p< 0.01$, significantly different from untreated cells; *$p<0.05$; **$p<0.01$, significantly different from treated cells at the same drug concentration.

Figure 4 Effect of CPT and CN-CPT on cells adhesion and cell migration of CAL-62 and BHT-101 cell lines. (A,B) HUVEC were treated or not treated with CPT or CN-CPT for 24 h, washed and used in the adhesion assay with untreated CAL-62 (A) and BHT-101 (B) cells (1×10^5/well). The data are presented as percentage of inhibition of the adhesion of treated cells compared to control (untreated cells). Each experiment was performed in triplicate. Data shown are means ± SEM (n = 5). *$p<0.05$; **$p<0.01$ significantly different from the same concentration of CPT. (C,D) In the Boyden chamber assay, CAL-62 (C) and BHT-101 (D) cells were plated onto the apical side of Matrigel-coated filters in the presence and absence of either CPT or CN-CPT, and FCS 20% was loaded in the basolateral chamber as a chemotactic stimulus. Data are expressed as mean ± SEM (n

= 5) of the percentage of inhibition versus control migration **p<0.01 significantly different from the same concentrations of CPT.

Figure 5 Effect of CPT and CN-CPT on ɓ-PIX expression and Erk1,2 phosphorylation in CAL -62 (A), and BHT-101 (C). Cells were treated with CPT or CN-CPT (10^{-8} and 10^{-9} M) for 48 h. CPT and CN-CPT were replenished every 24 h (48 h culture: 24 + 24 h) without changing the culture medium. The same blots were probed with anti ɓ-actin antibody as a control. (A, C): Western blot analysis from a representative experiment. (B, D): Densitometric analysis of ɓ-PIX expression and Erk1,2 phosphorylation expressed in arbitrary units; data are expressed as means ± SEM (n = 3) and shown as % of the controls. §p<0.05 significantly different from untreated cells; *p<0.05 significantly different from treated cells at the same concentration.

Figure 6 Treatment with CN-CPT delays the growth of orthotopic anaplastic thyroid carcinoma xenografts *in vivo*. CAL-62 cells ($1x10^6$) were injected into the right thyroid lobe of NSG mice. Mice were injected with PBS (ʒ, n = 5), CPT (ŏ, n = 7) or CN-CPT (□, n = 7) at day 10 after tumor challenge. (A) Kaplan-Meier survival analysis of untreated and treated mice. *p<0.05 compared to the PBS-treated group. Graphs show: (B) tumor velocity and (C) the number of metastasis in the lung for each group, expressed as median and interquartile range. *p<0.05; ***p<0.001 compared to the PBS-treated group and CPT- treated group. (D) Representative immunohystochemical staining for Ki-67 of tumor sections from mice treated with PBS, CPT or CN-CPT sacrificed at day 34 after tumor challenge. (E) Ki-67 staining of tumor section from a mouse treated with CN-CPT and sacrificed at day 51 after tumor challenge. (F) Graph shows the tumor microvessel density (TMD) determined as the percentage of CD31-positive area on the tumor sections. Three randomly selected areas from three tumors from each group were analysed; data are expressed as median and interquartile ranges. ***p<0.001 compared to the PBS-treated group and CPT- treated group.

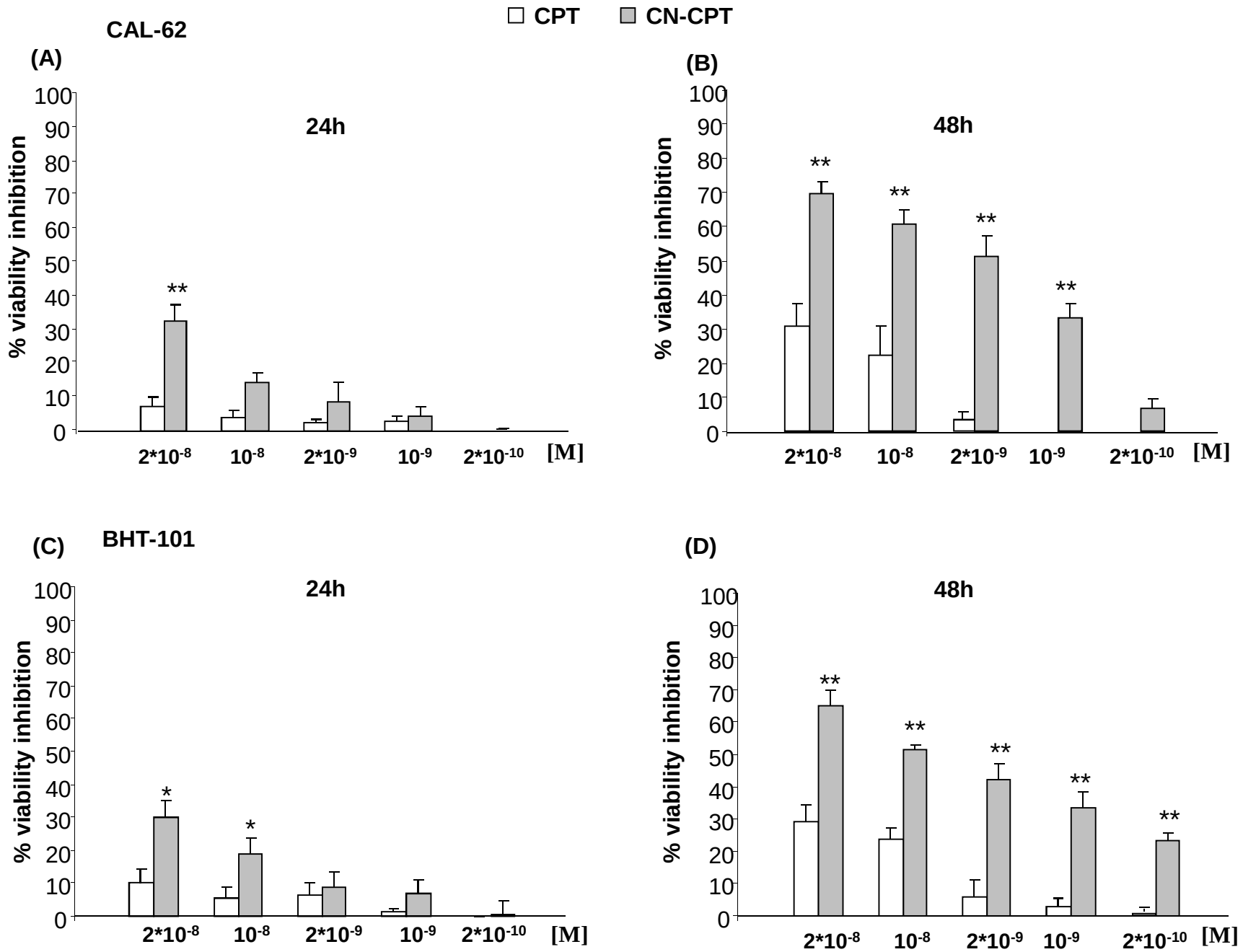
CPT
CN-CPT
CAL-62
(A)
24h
% viability inhibition
100
90
80
70
60
50
40
30
20
10
0
**
2*10-8
10-8
2*10-9
10-9
2*10-10
[M]
(B)
48h
**
**
**
**
BHT-101
(C)
24h
*
*
(D)
48h
**
**
**
**
**

Figure 1

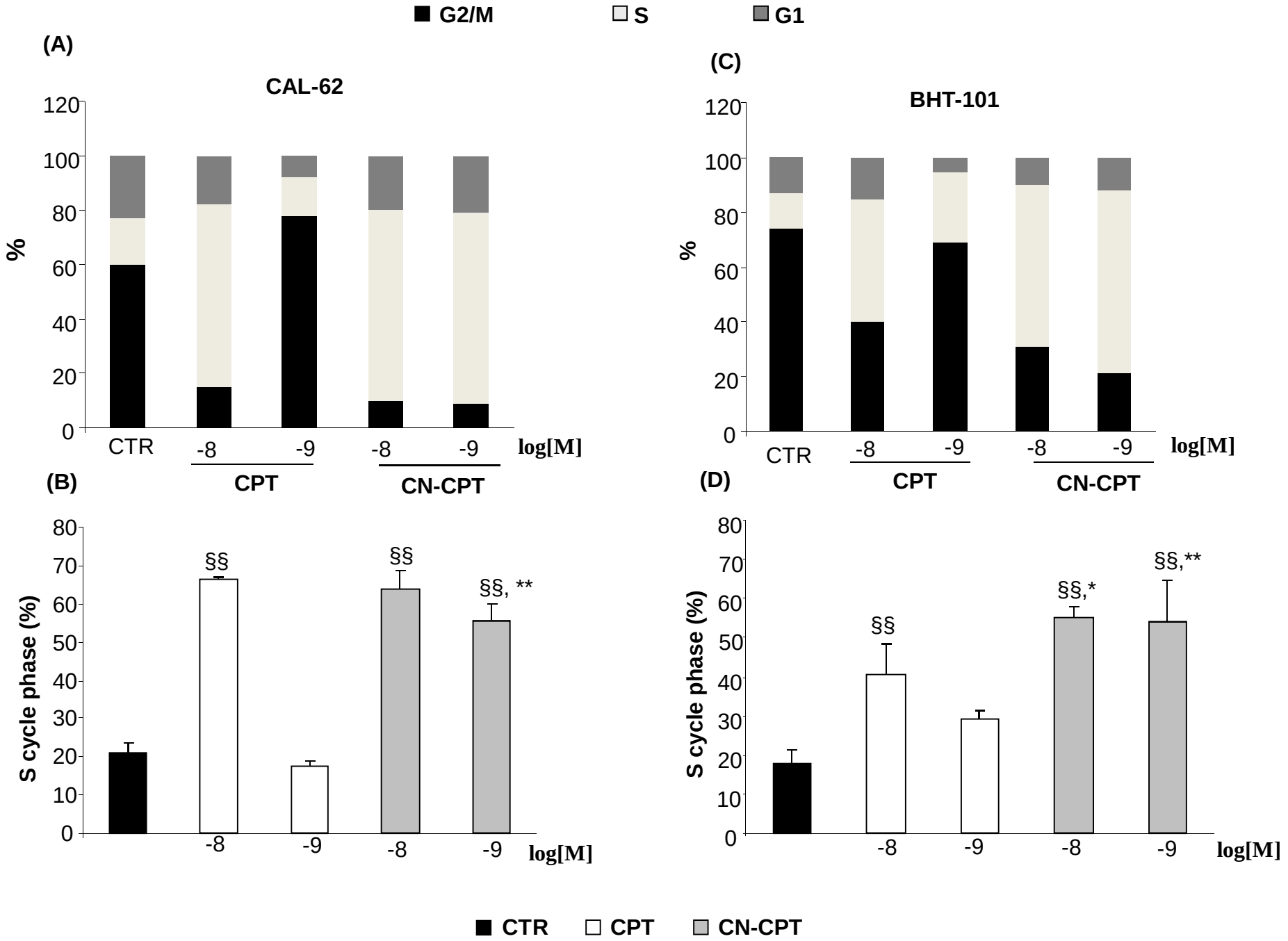
G2/M
S
G1
(A)
CAL-62
%
120
100
80
60
40
20
0
CTR
-8
-9
-8
-9
log[M]
CPT
CN-CPT
(C)
BHT-101
(B)
(D)
S cycle phase (%)
§§
§§, **
§§,*
§§,**
CTR
CPT
CN-CPT

Figure 2

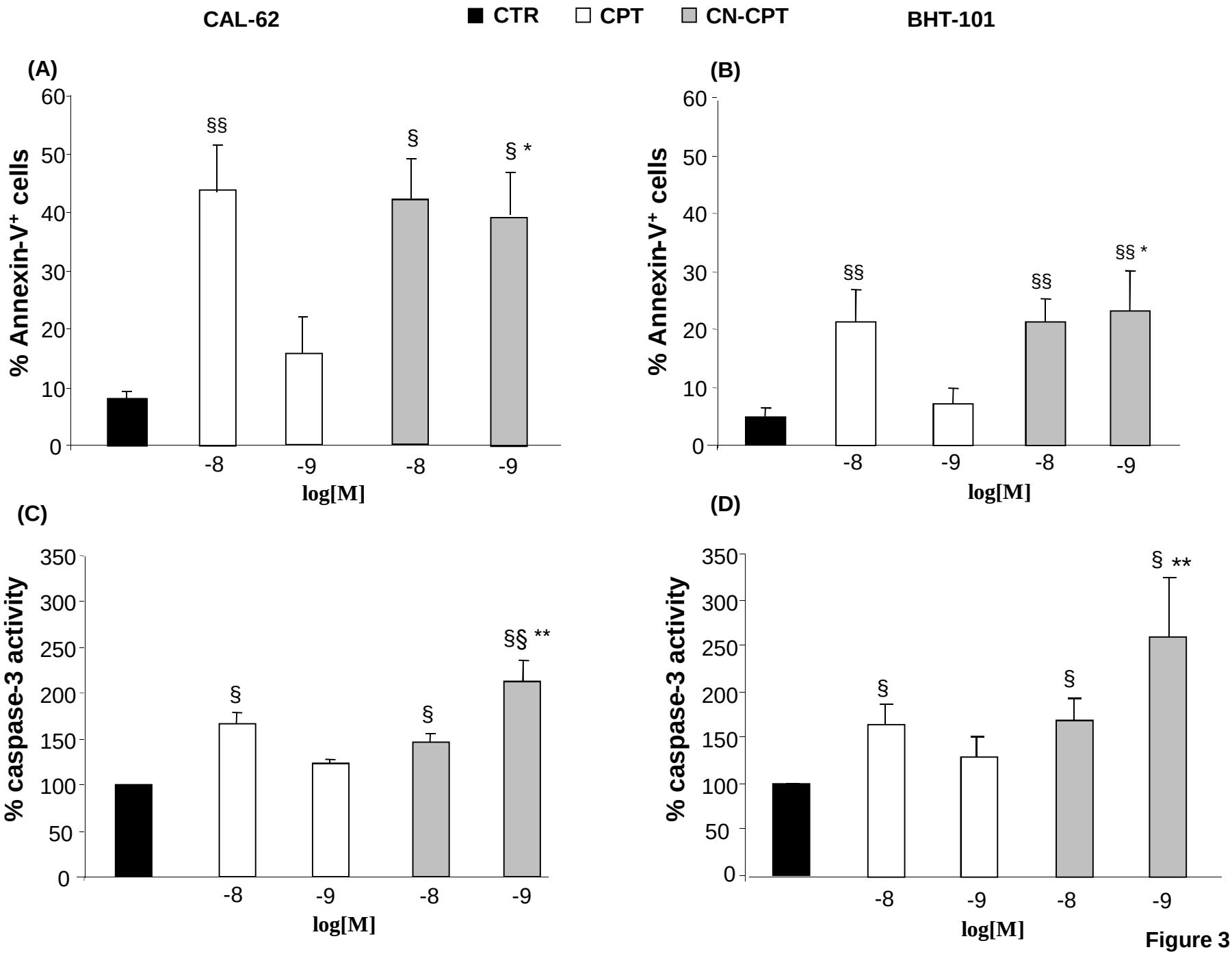
CAL-62
CTR
CPT
CN-CPT
BHT-101
(A)
% Annexin-V+ cells
60
50
40
30
20
10
0
§§
§
§ *
-8
-9
-8
-9
log[M]
(B)
% Annexin-V+ cells
60
50
40
30
20
10
0
§§
§§
§§ *
-8
-9
-8
-9
log[M]
(C)
% caspase-3 activity
350
300
250
200
150
100
50
0
§
§
§§ **
-8
-9
-8
-9
log[M]
(D)
% caspase-3 activity
350
300
250
200
150
100
50
0
§
§
§ **
-8
-9
-8
-9
log[M]

Figure 3

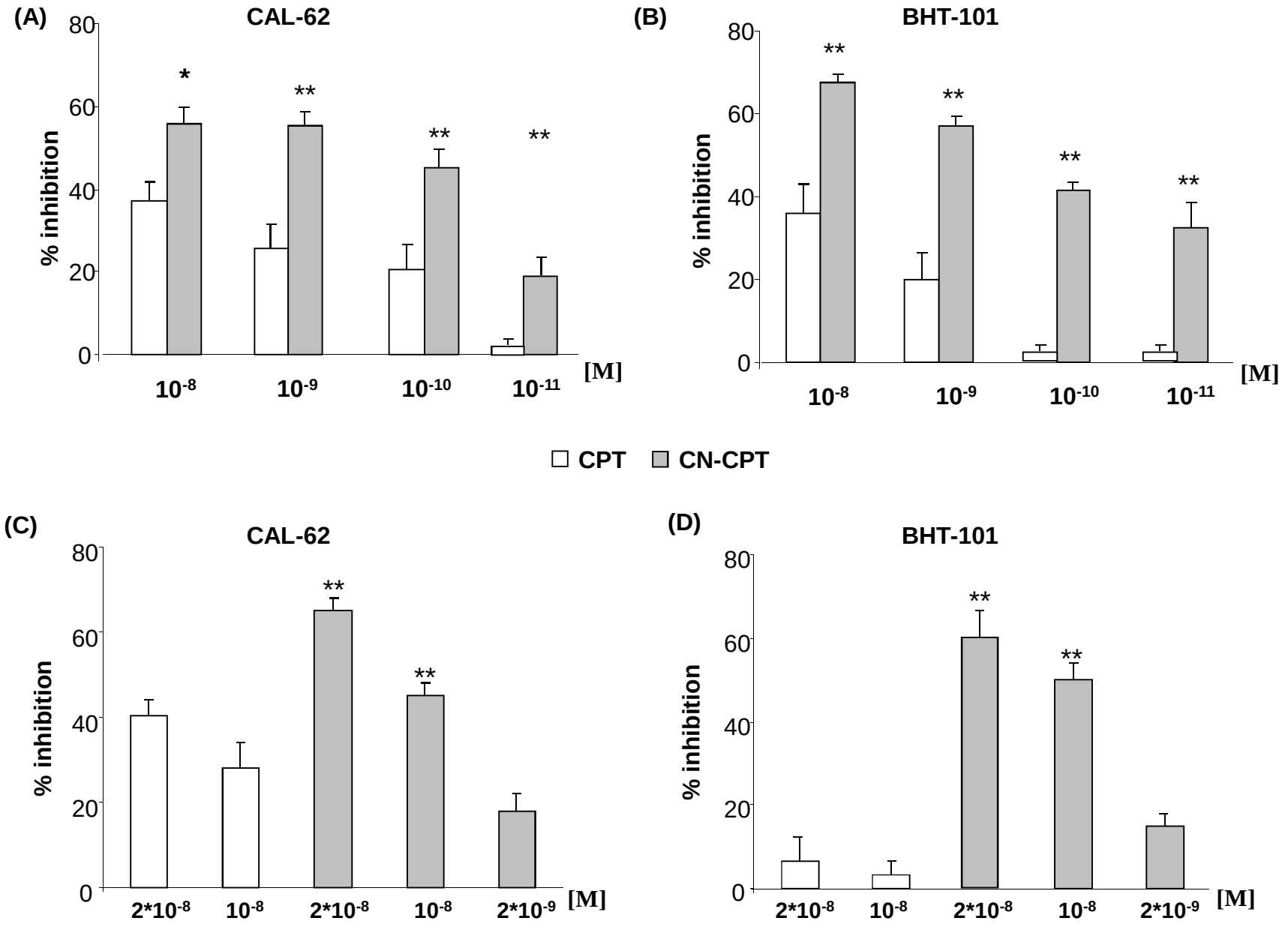
(A)
CAL-62
% inhibition
0
20
40
60
80
*
**
**
**
10-8
10-9
10-10
10-11
[M]
(B)
BHT-101
% inhibition
0
20
40
60
80
**
**
**
**
10-8
10-9
10-10
10-11
[M]
CPT
CN-CPT
(C)
CAL-62
% inhibition
0
20
40
60
80
**
**
2*10-8
10-8
2*10-8
10-8
2*10-9
[M]
(D)
BHT-101
% inhibition
0
20
40
60
80
**
**
2*10-8
10-8
2*10-8
10-8
2*10-9
[M]

Figure 4

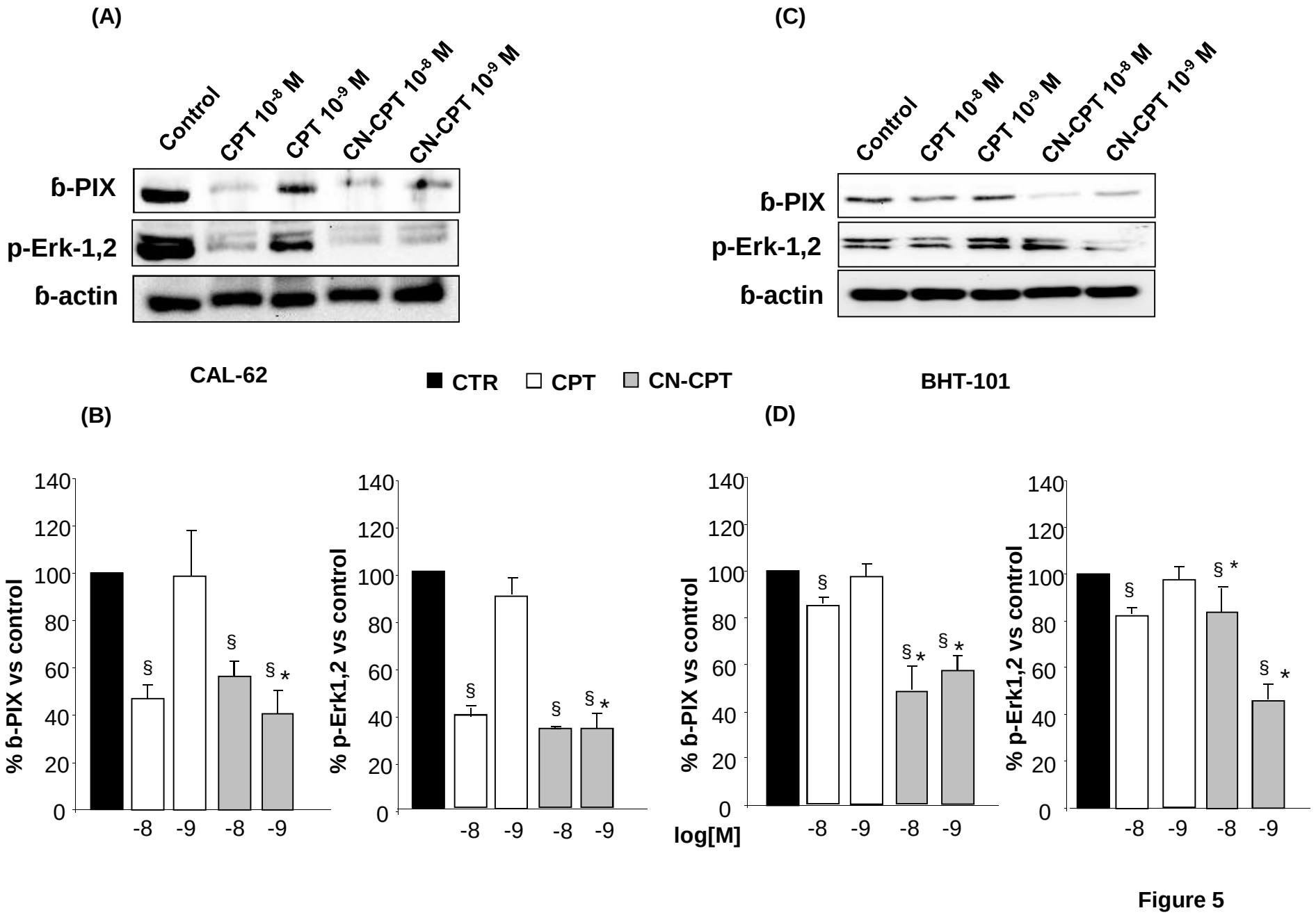
(A)
Control
CPT 10-8 M
CPT 10-9 M
CN-CPT 10-8 M
CN-CPT 10-9 M
ß-PIX
p-Erk-1,2
ß-actin
(C)
Control
CPT 10-8 M
CPT 10-9 M
CN-CPT 10-8 M
CN-CPT 10-9 M
ß-PIX
p-Erk-1,2
ß-actin
CAL-62
CTR
CPT
CN-CPT
BHT-101
(B)
% ß-PIX vs control
% p-Erk1,2 vs control
(D)
% ß-PIX vs control
% p-Erk1,2 vs control
log[M]
-8
-9

Figure 5

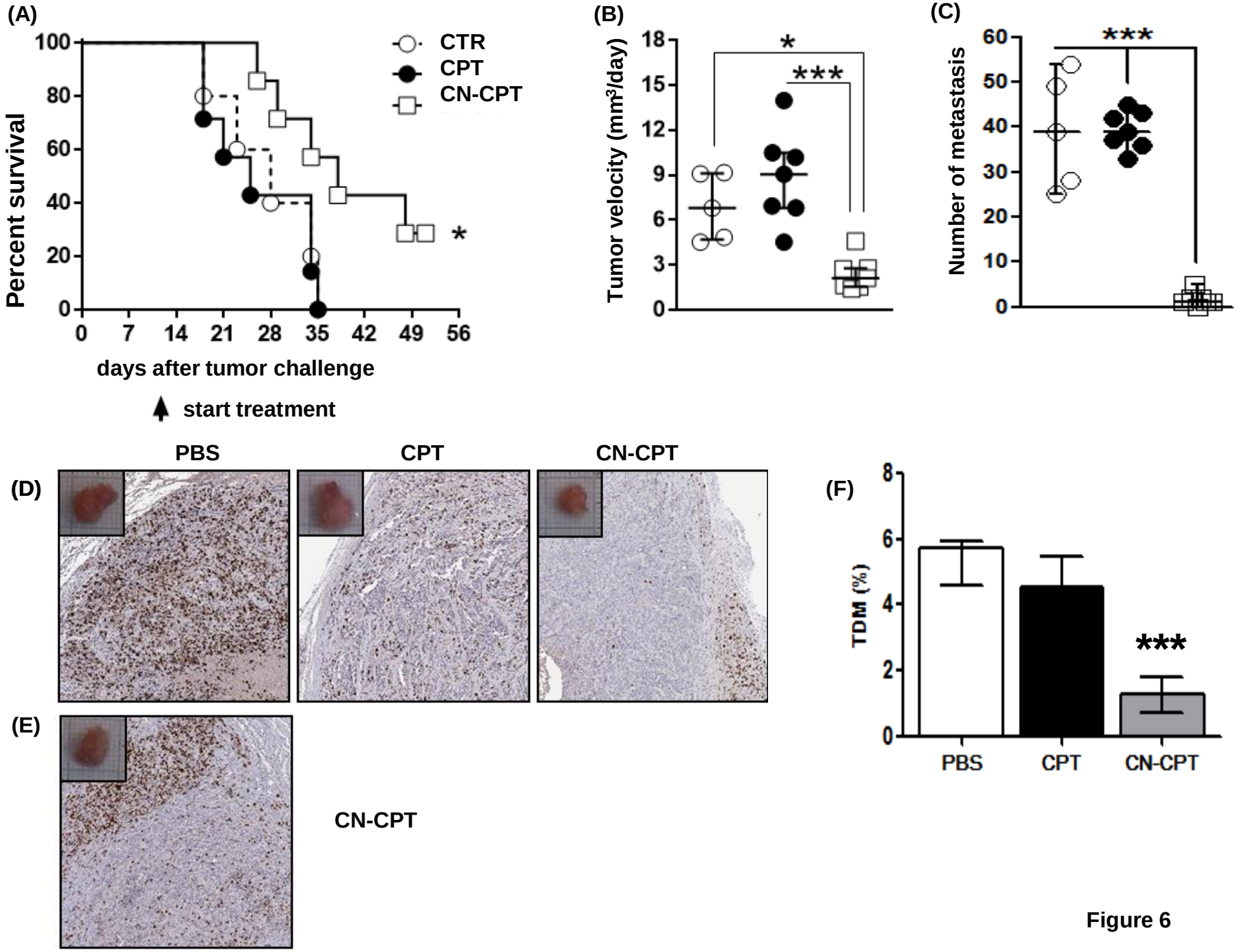
(A)
Percent survival
100
80
60
40
20
0
0 7 14 21 28 35 42 49 56
days after tumor challenge
CTR
CPT
CN-CPT
*
start treatment
(B)
Tumor velocity (mm³/day)
18
15
12
9
6
3
0
*
***
(C)
Number of metastasis
60
50
40
30
20
10
0
***
PBS
CPT
CN-CPT
(D)
(E)
CN-CPT
(F)
TDM (%)
8
6
4
2
0
***
PBS
CPT
CN-CPT

Figure 6

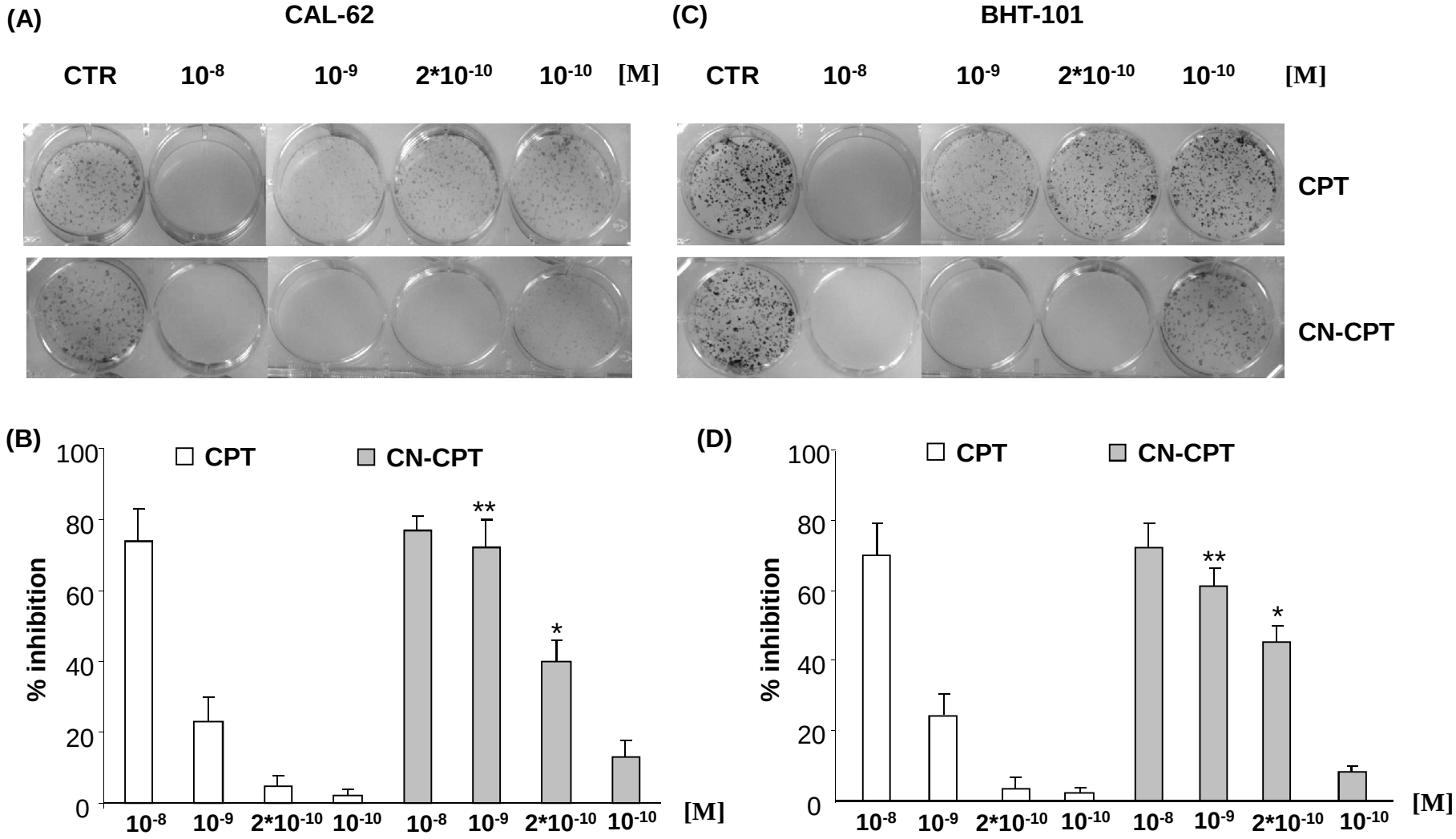

Figure S1: Effect of CPT and CN-CPT on cell clonogenicity was tested by the colony forming assay. CAL-62 (A, B) and BHT-101 (C, D) cells (800/well) were seeded in six-well plates and treated with each drug formulation at the indicated concentrations for 72 h. The medium was then changed and cells were cultured for an additional 10 days and subsequently fixed and stained with crystal violet. (A, C) Photographs of the fixed plates from a representative experiment. (B, D) Clonogenicity inhibition % (compared to controls) expressed as means ± SEM (n = 5). *P < 0.05, **P < 0.01 significantly different from the same concentration of CPT.

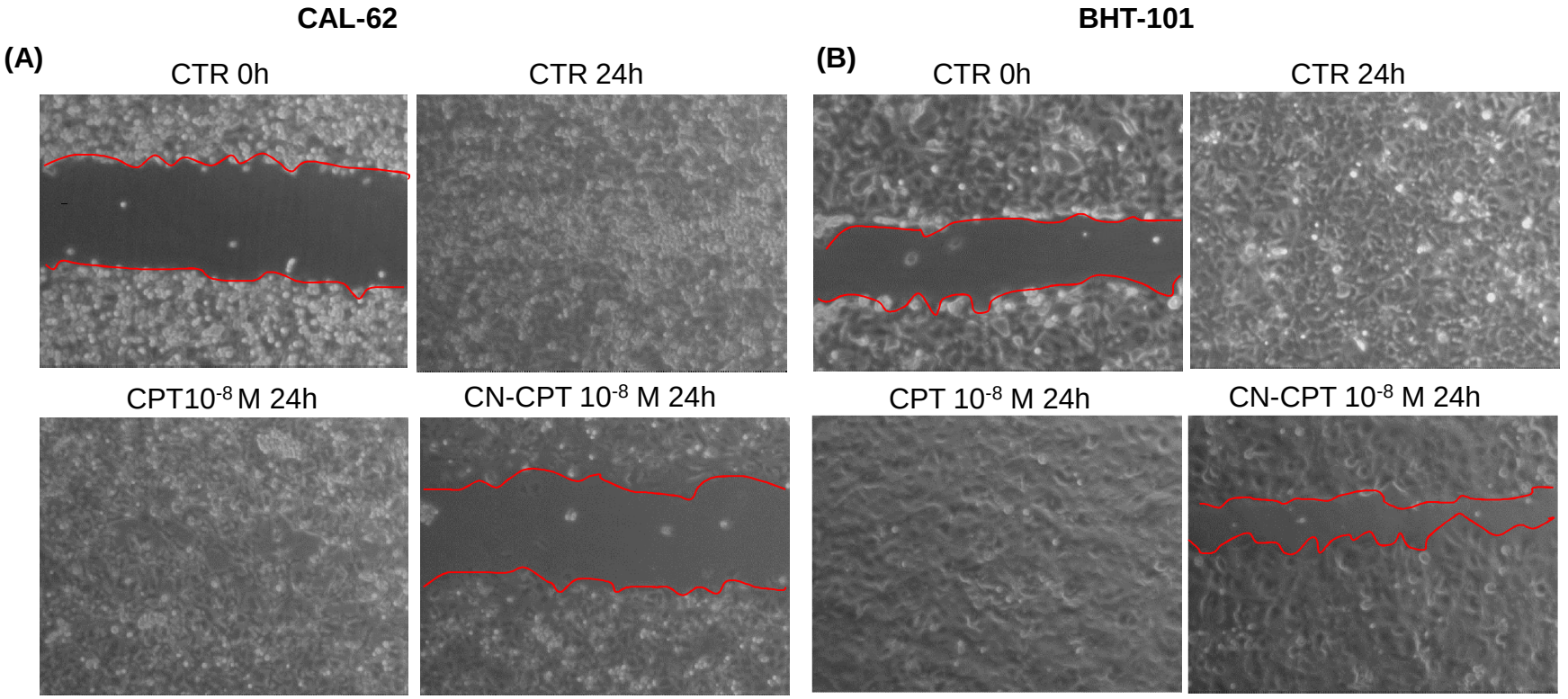

Figure S2: Effect of CPT and CN-CPT on motility of CAL-62 and BHT-101 cell lines assessed using the wound healing assay. A scratch was made through CAL-62 (A) and BHT-101 (B) cell layer and then cells were cultured in the presence and absence of CPT or CN-CPT for 24 h. Microphotographs of the wounded area were taken immediately after the scratch (0 h) and 24 h later, in order to monitor cell migration into the wounded area (n = 3).